Age-dependent mortality, fecundity and mobility effects on front speeds: theory and application to the Neolithic transition

J. Stat. Mech. (2010) P11006

(http://iopscience.iop.org/1742-5468/2010/11/P11006)

Journal of Statistical Mechanics: Theory and Experiment
An IOP and SISSA journal

Age-dependent mortality, fecundity and mobility effects on front speeds: theory and application to the Neolithic transition

Joaquim Pérez-Losada and Joaquim Fort

Complex Systems Laboratory, Departament de Física, Universitat de Girona, 17071 Girona, Catalonia, Spain
E-mail: joaquim.perez@udg.edu and joaquim.fort@udg.edu

Received 29 July 2010
Accepted 7 October 2010
Published 2 November 2010

Online at stacks.iop.org/JSTAT/2010/P11006
doi:10.1088/1742-5468/2010/11/P11006

Abstract. We present a model that makes it possible to analyze the effect of the age dependences of mortality, fertility and dispersal persistence on the speed of propagating fronts in two spatial dimensions. Speeds derived analytically agree very well with those obtained from numerical simulations. Infant mortality and total fecundity are the most relevant parameters affecting the front speed, whereas the adult mortality rates and dispersal persistences are less important. We apply the model to the Neolithic transition in Europe. The predictions of the model are consistent with the archaeological data for the front speed, provided that the infant mortality lies within a relatively narrow range.

Keywords: population dynamics (theory)

J. Stat. Mech. (2010) P11006

1742-5468/10/P11006+13$30.00

Contents

1. Introduction

Reaction–dispersal front propagation models have been applied to investigate many systems, such as human invasions [1, 2], virus infections [3], tree colonizations [4], flame propagation [5, 6], etc (for some reviews, see [7]–[10]).

A variety of models have been developed in recent years for analyzing the speeds of human invasion fronts. Earlier models were based on the equation

$$p(x,y,t+T)-p(x,y,T)=\int_{-\infty}^{+\infty}\int_{-\infty}^{+\infty}p(x+\Delta_x,y+\Delta_y,t)\,\phi(\Delta_x,\Delta_y)\,\mathrm{d}\Delta_x\,\mathrm{d}\Delta_y - p(x,y,T)+R[p(x,y,t)], \tag{1}$$

where $p(x,y,t+T)$ is the population density at the location (x,y) and time $t+T$. The time interval T is that between two subsequent dispersal events or 'jumps', i.e. one generation (defined as the mean age difference between an individual and her/his children). The dispersal kernel $\phi(\Delta_x,\Delta_y)$ is the probability per unit area that the children of an individual located at $(x+\Delta_x,y+\Delta_y,t)$ become adults at $(x,y,t+T)$. The first term on the right-hand side of equation (1) corresponds to population dispersal and the last one, $R[p(x,y,t)]$, to net reproduction (births minus deaths). For isotropic kernels, equation (1) can be Taylor expanded up to second order in space and first order in time to yield Fisher's equation [11, 12],

$$\partial p/\partial t = D\nabla^2 p + F(p) \tag{2}$$

where $D \equiv (1/4T)\int_{-\infty}^{+\infty}\int_{-\infty}^{+\infty}\phi(\Delta_x,\Delta_y)\left(\Delta_x^2+\Delta_y^2\right)\mathrm{d}\Delta_x\,\mathrm{d}\Delta_y$ is the diffusion coefficient and $F(p)\equiv\partial R/\partial t$ is called the population growth function. In Fisher's equation a logistic form is assumed, $F(p)=ap(1-p/p_{\max})$ (a is called the initial growth rate and $p_{\max}$ the carrying capacity). If the Taylor expansion is performed up to second order, time-delayed models are obtained instead [1, 13].

According to equation (1), newborn individuals can appear at (x,y) (last term) while their parents migrate away from (x,y) (the first term on the right-hand side). In other words, according to those models parents can leave their newborn children alone. However, newborn humans cannot survive alone without their parents during a substantial time. For this reason, in recent years it has been proposed that the following equation is more

J. Stat. Mech. (2010) P11006

realistic than equation (1) for human populations (for some detailed derivations, see equation (10) in [14], equation (4) and figure 1 in [15], and equation (176) and figure 17 in [9]),

$$p(x, y, t+T) = R_0 \int_{-\infty}^{+\infty} \int_{-\infty}^{+\infty} p(x+\Delta_x, y+\Delta_y, t)\, \phi(\Delta_x, \Delta_y)\, \mathrm{d}\Delta_x\, \mathrm{d}\Delta_y, \tag{3}$$

where R_0 is the net fecundity or reproductive rate. This is a net rate, i.e. it also includes mortality effects. Therefore, R_0 is the mean number of reproductive children per parent (here reproductive means not just fertile, but that they will eventually reproduce). In practice, R_0 is estimated by the ratio of the number of individuals at a given time divided by the number of individuals a generation time T earlier [14].

Equation (3) is valid only at sufficiently low values of the population density p, because there is a maximum saturation density $p_{\max}$ above which net reproduction vanishes. For this reason, this model applies the simple cut-off $p(x, y, t+T) = p_{\max}$ in the case where equation (3) yields $p(x, y, t+T) > p_{\max}$ [14].

In principle, instead of equation (3) and this cut-off, one might be tempted to use a logistic finite-difference equation,

$$p(x, y, t+T) = R_0 \widetilde{p} \left(1 - \frac{\widetilde{p}}{p_{\max}}\right), \tag{4}$$

with $\widetilde{p} = \int_{-\infty}^{+\infty} \int_{-\infty}^{+\infty} p(x+\Delta_x, y+\Delta_y, t)\, \phi(\Delta_x, \Delta_y)\, \mathrm{d}\Delta_x\, \mathrm{d}\Delta_y$. However, we will not apply equation (4) because it is known from non-spatial models that it can yield negative values for $p(x, y, t+T)$ for some values of R_0 [16, 17] (in contrast, the logistic differential-equation model, i.e. Fisher's equation (2), does not have this problem, but it is also unsuitable because it cannot take into account three important effects: the delay time [1, 13], the dispersal kernel shape [15, 18] and, as explained above, the cohabitation of children and their parents [9, 14, 15]). Equations (3) and (4) differ in the saturation behavior, i.e. in the way in which the population density p approaches its upper limit $p_{\max}$. However, this is not important because the saturation behavior has not been observed in natural populations outside the laboratory [19]. Moreover, both equations (4) and (3) imply an exponential increase at low values of p, so the speeds of fronts are the same in the two models. Indeed, we have checked by means of numerical integrations that the front speeds predicted by equations (4) and (3) differ by less than 0.3% for the realistic values of the reproductive rate ($1.9 < R_0 < 2.6$) and the dispersal kernel introduced in [14]. Therefore, both equations (4) and (3) yield the same front speeds, but conceptually we find equation (3) more reasonable than (4), because the latter can yield negative values of the population density in some circumstances [16, 17].

Equation (3) is called the non-overlapping generation model. Note that in this model, all traits in the life history of the individuals are ignored, i.e. only the age-independent parameters T and R_0 are used. Therefore, this model cannot analyze any effect on the front speed of the fact that the fecundity, mortality and dispersal kernel depend on the age of individuals. In this paper, we will extend this model to allow for such dependences. Previously, age-dependent models have been built for one-dimensional range expansions [20]–[22] and, more recently, for the spread of epidemics [23]. A model also exists for tree population range expansions [24] but, as we shall explain below, such a model cannot be applied to human populations.

J. Stat. Mech. (2010) P11006

In section 2 we present a generalization of the model (3), and in section 3 we test the results using numerical simulations. Section 4 is devoted to the application of our new model to the Neolithic transition in Europe, and section 5 summarizes our conclusions.

Before presenting our model, it is worth mentioning that noise can affect front propagation rates under certain conditions. This effect appears at low enough particle numbers [25, 26], but for Neolithic transition fronts it has been shown recently that such stochastic effects are not important, due to the fact that the carrying capacity of pre-industrial farming populations is large enough to make such effects negligible (see section 6 in [15]).

2. The theoretical model

In order to take into account the dependences of fecundity, mortality and dispersal on age, we regard the population as subdivided into several age groups. For simplicity, and also for later application to data appropriate to the Neolithic transition (section 4), we consider only four groups (however, all of our results can be easily extended to an arbitrarily large number of groups). For definiteness, let the age group subindices be ordered so that $p_1(x, y, t)$ corresponds to the youngest age group and $p_4(x, y, t)$ to the oldest one. Then we generalize equation (3) into the set

$$\begin{aligned}
p_1(x,y,t+\tau) &= f_2 \int \phi_2(\Delta_x,\Delta_y) p_2(x+\Delta_x, y+\Delta_y, t)\,\mathrm{d}\Delta_x\,\mathrm{d}\Delta_y \\
&\quad + f_3 \int \phi_3(\Delta_x,\Delta_y) p_3(x+\Delta_x, y+\Delta_y, t)\,\mathrm{d}\Delta_x\,\mathrm{d}\Delta_y \\
&\quad + f_4 \int \phi_4(\Delta_x,\Delta_y) p_4(x+\Delta_x, y+\Delta_y, t)\,\mathrm{d}\Delta_x\,\mathrm{d}\Delta_y \\
p_2(x,y,t+\tau) &= (1-m_1) \int \phi_1(\Delta_x,\Delta_y) p_1(x+\Delta_x, y+\Delta_y, t)\,\mathrm{d}\Delta_x\,\mathrm{d}\Delta_y \\
p_3(x,y,t+\tau) &= (1-m_2) \int \phi_2(\Delta_x,\Delta_y) p_2(x+\Delta_x, y+\Delta_y, t)\,\mathrm{d}\Delta_x\,\mathrm{d}\Delta_y \\
p_4(x,y,t+\tau) &= (1-m_3) \int \phi_3(\Delta_x,\Delta_y) p_3(x+\Delta_x, y+\Delta_y, t)\,\mathrm{d}\Delta_x\,\mathrm{d}\Delta_y
\end{aligned} \tag{5}$$

where $p_i(x, y, t)$ is the population density (number of individuals per unit area) of age group i, f_i is its fecundity, m_i its mortality, and $\phi_i(\Delta_x, \Delta_y)$ its dispersal kernel. We assume that the infant population $p_1(x, y, t)$ does not reproduce, so $f_1 = 0$ in equations (5) (this is in agreement with the data that we will use in section 4). The time interval τ should be chosen so that the demographic data on mortality, fecundity and dispersal, which are always recorded in age intervals, can be applied to equations (5) (see section 3). Like for the age groups with densities p_1, p_2 and p_3, mortality will also affect the dynamics of subpopulation p_4, but this effect is not included in equations (5) for the following reason. Since by definition p_4 is the oldest age group, all individuals corresponding to p_4 will simply disappear after their reproduction and dispersal, and their death will not affect the front speed (this will be checked by the agreement between our model in this section and the simulations in section 3, where the mortality of subpopulation p_4 is explicitly included).

J. Stat. Mech. (2010) P11006

It is important to stress that the form of the evolution equations (equations (5) in our case) is highly dependent on the biological properties of the species considered. Indeed, the integrals of dispersal kernels over all space appear in each of our equations (5) because we are here dealing with human populations, whereas for tree populations a dispersal kernel appears only in the evolution equation for p_1 because in that case the dispersal takes place only for seeds and not for trees [24].

Before deriving the theoretical speed for our model, let us stress that all of the equations in the former set (5) will be used in our numerical simulations (section 3) using values appropriate to a specific application, namely the Neolithic transition. As we shall see in section 3, then the appropriate age interval is $\tau = 12.5$ yr and $f_4 = 0$ according to the ethnographic data available. The latter value ($f_4 = 0$) can be used to make our theoretical equations (5) much simpler, if we predict intuitively that the fact that the oldest population $p_4(x, y, t)$ does not reproduce ($f_4 = 0$) will make it totally irrelevant to the propagation speed of the invasion front. Under this assumption, that will be checked in section 3 by means of numerical simulations of the whole set (5), the system (5) reduces to

$$\begin{aligned} p_1(x,y,t+\tau) &= f_2 \int \phi_2(\Delta_x,\Delta_y) p_2(x+\Delta_x, y+\Delta_y, t)\,\mathrm{d}\Delta_x \mathrm{d}\Delta_y \\ &\quad + f_3 \int \phi_3(\Delta_x,\Delta_y) p_3(x+\Delta_x, y+\Delta_y, t)\,\mathrm{d}\Delta_x\,\mathrm{d}\Delta_y \\ p_2(x,y,t+\tau) &= (1-m_1) \int \phi_1(\Delta_x,\Delta_y) p_1(x+\Delta_x, y+\Delta_y, t)\,\mathrm{d}\Delta_x\,\mathrm{d}\Delta_y \\ p_3(x,y,t+\tau) &= (1-m_2) \int \phi_2(\Delta_x,\Delta_y) p_2(x+\Delta_x, y+\Delta_y, t)\,\mathrm{d}\Delta_x\,\mathrm{d}\Delta_y. \end{aligned} \tag{6}$$

In order to derive the asymptotic front speed, we look for constant-shape solutions for each subpopulation, i.e. $p_i(x, y, t) = w_i \exp[-\lambda(x - ct)]$ $(i = 1, 2, 3)$ in the limit in which the coordinate co-moving with the front $z \equiv x - ct \to \infty$. Then the set of equations (5) becomes

$$\begin{aligned} w_1 \exp(\lambda c) &= f_2 w_2 \int_0^\infty \varphi_2(\Delta) I_0(\lambda\Delta)\Delta\,\mathrm{d}\Delta + f_3 w_3 \int_0^\infty \varphi_3(\Delta) I_0(\lambda\Delta)\Delta\,\mathrm{d}\Delta \\ w_2 \exp(\lambda c) &= (1-m_1) w_1 \int_0^\infty \varphi_1(\Delta) I_0(\lambda\Delta)\Delta\,\mathrm{d}\Delta \\ w_3 \exp(\lambda c) &= (1-m_2) w_2 \int_0^\infty \varphi_2(\Delta) I_0(\lambda\Delta)\Delta\,\mathrm{d}\Delta, \end{aligned} \tag{7}$$

where

$$I_0(\lambda\Delta) \equiv \frac{1}{2\pi} \int_0^{2\pi} \mathrm{d}\theta \exp\left[\lambda\Delta\cos\theta\right] \tag{8}$$

is the modified Bessel function of the first kind and order zero, and we have assumed that the ϕ_i depend only on distance $\Delta \equiv \sqrt{\Delta_x^2 + \Delta_y^2}$ (isotropic kernels). The dispersal probability per unit area $\phi_i(\Delta)$ is related to that per unit length $\varphi_i(\Delta)$ (i.e. into a 2D ring of area $2\pi\Delta\,\mathrm{d}\Delta$) as $\varphi_i(\Delta) = 2\pi\Delta\phi_i(\Delta)$ [4].

For simplicity, let us assume a simple description in which

$$\phi_i(\Delta) = p_{ei}\delta^{(2)}(\Delta) + (1 - p_{ei})\delta^{(2)}(\Delta - r) \tag{9}$$

where $\delta^{(2)}$ is the two-dimensional Dirac delta function, i.e., an individual of age group i either stays at rest (with probability p_{ei}, which is called the persistence of age group i) or moves distance r (with probability $1-p_{ei}$). Such a description has been useful previously in several models [14, 15, 27] that did not take the age structure of the population into account. In those papers it was also shown that a realistic value for the mobility distance of prehistoric human populations is $r = 50$ km. We use a single value for r because using a different value for each age group would substantially complicate the simulations in section 3. We think that this is reasonable because in our model the value of the persistence p_{ei} (and, therefore, the mobility behavior of the individuals) is allowed to depend on age. Then, using matrix notation, the system (7) can be rewritten as

$$\exp(\lambda c)\vec{w} \equiv \overrightarrow{\overrightarrow{H}}(\lambda)\vec{w}, \tag{10}$$

where we have defined

$$\vec{w} \equiv \begin{pmatrix} w_1 \\ w_2 \\ w_3 \end{pmatrix}, \tag{11}$$

$$\overrightarrow{\overrightarrow{H}}(\lambda) \equiv \begin{pmatrix} 0 & f_2\Psi_2(\lambda) & f_3\Psi_3(\lambda) \\ (1-m_1)\Psi_1(\lambda) & 0 & 0 \\ 0 & (1-m_2)\Psi_2(\lambda) & 0 \end{pmatrix}, \tag{12}$$

and

$$\Psi_i(\lambda) \equiv p_{ei} + (1-p_{ei})I_0(\lambda r). \tag{13}$$

As usual, according to marginal stability analysis [28] the front speed c for systems with the form (10) can be found from the well-known expression [20]

$$c = \min_{\lambda} \frac{1}{\lambda}\rho_1(\lambda), \tag{14}$$

with ρ_1 the largest of the eigenvalues of $\overrightarrow{\overrightarrow{H}}(\lambda)$.

3. Numerical simulations

The numerical simulations of the system (5) are performed on a 2D grid with 1000×1000 nodes, with nearest-neighbor distance $r = 50$ km (see section 2). Initially $p_i(x, y, t) = 0.25$ (but the front speed does not depend on these values) for $i = 1, \ldots, 4$ at the central node, and 0 elsewhere. At each time interval, corresponding to $\tau = 12.5$ yr, we compute the new subpopulation number densities $p_i(x, y, t + \tau)$ at all nodes of the 2D grid in a two-step process: dispersal and growth (the latter includes reproduction and deaths). In the dispersal step, as in the analytical model in section 2, a fraction p_{ei} of the population in age group i stays at the original node, and the remaining fraction is distributed equally among the nearest neighbors, i.e., a fraction $(1-p_{ei})/4$ jumps a distance $\pm r$ along each horizontal or vertical direction. In the second step, the effects of reproduction and mortality are computed as follows. At each node, the new infant population density p_1 is computed as $\sum_{i=2}^{4} f_i p_i$ (see the first equation in the set (5); the numerical values of f_i are given below). The new population density p_i for each of the remaining three age groups ($i = 2, \ldots, 4$)

J. Stat. Mech. (2010) P11006

Table 1. Model parameters and their ranges.

Parameter (units)	Characteristic value	Minimum value	Maximum value	References
F (children/adult)	3.30	3.00	3.50	[29, 30]
m_1 (dimensionless)	0.55	0.27	0.77	[32]
m_2 (dimensionless)	0.30	0.15	0.45	[32]
m_3 (dimensionless)	0.40	0.20	0.60	[32]
m_4 (dimensionless)	1.00	1.00	1.00	[32]
p_{e1} (dimensionless)	0.38	0.19	0.54	[33]
p_{e2} (dimensionless)	0.38	0.19	0.54	[33]
p_{e3} (dimensionless)	0.38	0.19	0.54	[33]
p_{e4} (dimensionless)	0.38	0.19	0.54	[33]

is computed by removing a fraction $m_{i-1}p_{i-1}$ from the population density p_{i-1} (see the last three equations in the set (5)). In order to avoid an unbounded population growth, if after any of these steps a population density in a grid node exceeds the saturation value, then it is set equal to the saturation value (we used a saturation value of unity in our simulations, $p_{\max} = 1$ individual km^{-2}, but changing it does not modify the front speed). The two-step dispersal–growth cycle is then repeated many times, until a constant speed for the propagation of the population profiles is reached (we define the position of the front as that with $p_1 = 0.05$, but the value of the speed obtained does not depend on this definition).

The mean observed values of the parameters, as well as the ranges used in the simulations, are reported in table 1. They have been obtained as follows. First, as mentioned above, in order to use the histograms for the fecundities in [29, 30], the appropriate interval between age groups is $\tau = 12.5$ yr. From table 2 in [29], the characteristic value for the total fertility ratio F of pre-industrial agriculturalists was estimated as $F \simeq 6.6$ children per adult woman. The characteristic value $F \simeq 3.3$ children per adult is given in our table 1 in the units appropriate for use in our model (this is half the value per adult woman, because the number of women and men in human populations are approximately the same). An upper bound for F was set to 7.0 children per adult woman (from the estimations for Linearbandkeramik (LBK) farmers during their range expansion in Western Europe [31]). The minimum value for pre-industrial agriculturalists is $F = 6.0$ children per adult woman, according to table 2 in [29]. The age-dependent fecundities f_i used in our model were estimated by multiplying the total fertility F by the age-specific relative ratios (defined as the age-specific rate f_i divided by the total rate F) in natural fertility populations, as given in [30], figure 2.5. For $F = 3.3$ children per adult, this yields $f_1 = 0.0$, $f_2 = 2.3$, $f_3 = 1.0$, $f_4 = 0.0$ children per adult. Age-dependent mortalities were estimated from table 4 in [32], yielding the characteristic values $m_1 = 0.55$, $m_2 = 0.30$, $m_3 = 0.40$, $m_4 = 1.00$. Finally [33], is the only source that we know of with quantitative dispersal data for pre-industrial agriculturalist populations. Unfortunately, it does not seem possible to estimate the age-dependent persistences p_{ei} because all mobility data give individual distances moved since birth, not since the individual had several specific ages. However, [33] makes it possible to estimate several values of the persistence of the individuals in the youngest age group, p_{e1}. As noted in a previous publication [14], the mean is $p_{e1} = 0.38$ and the range is $0.19 \leq p_{e1} \leq 0.54$. Due to the lack of more refined

J. Stat. Mech. (2010) P11006

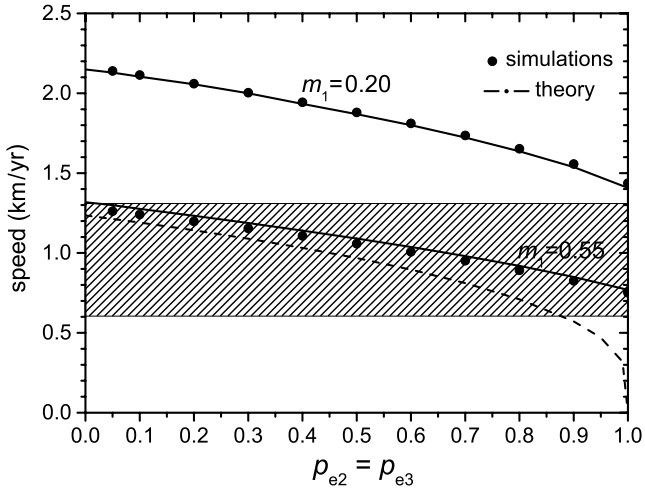

Figure 1. Front speed in 2D versus adult dispersion persistence, for two values of the infant mortality. The hatched region gives the observed range for the Neolithic front speed [34]. The numerical results for the model with several age groups (circles) agree well with the analytical results for the same model (full curves). Note that for an infant mortality $m_1 = 0.55$, which has been derived from data for real populations [32], any value of $p_{e2} = p_{e3}$ yields a speed consistent with the data. We have used $f_1 = 0.0$, $f_2 = 2.3$, $f_3 = 1.0$, $f_4 = 0.0$, $m_2 = 0.30$, $m_3 = 0.40$, $m_4 = 1.00$ and $p_{e1} = 0.38$ (see section 3). The dashed curve corresponds to the single-population model of equation (3), i.e. to neglecting any dependence of fertility, mortality or persistence on age (this curve has been computed using equation (14) in [14] and the mean values derived from anthropological observations in that reference, namely $R_0 = 2.2$, $T = 32$ yr and $r = 50$ km).

information, we approximated the persistences of older individuals (p_{e2}, p_{e3} and p_{e4}) to the same range as that of p_{e1} (table 1). In fact, we will find that our model is consistent with the data for any value of these persistences (figure 1).

4. Application to the Neolithic transition in Europe

Finally we can apply our model to the Neolithic transition in Europe. In figure 1, the full lines are the analytical results from equation (14), and the symbols have been obtained using the numerical simulations described in the previous section. In figure 1, the persistence of the youngest population has its characteristic value, $p_{e1} = 0.38$ (table 1), and we have assumed $p_{e2} = p_{e3}$ (because, as mentioned above, only p_{e1} can be reliably estimated from the ethnographic data available; p_{e2} and p_{e3} cannot). The persistence of the oldest age group, p_{e4}, does not have any effect on the front speed (simply because it appears only in the term multiplying $f_4 = 0$ in equations (5)). The hatched rectangle in figure 1 corresponds to the speed range of the Neolithic transition in Europe, as determined from archaeological data (0.6–1.3 km yr^{-1}) [34].

From figure 1 we see that the infant mortality m_1 has a very important effect on the front speed. Indeed, the predicted speeds are consistent with the observed range (hatched rectangle) for an infant mortality of $m_1 = 0.55$ (such a value has been estimated

J. Stat. Mech. (2010) P11006

from the age determination of Neolithic skeletons; see e.g. table 4 in [32]). However, the predicted speeds are totally inconsistent with the observed range for other values of the infant mortality, e.g. for $m_1 = 0.20$. From figure 1 we conclude that (i) the predictions of the model are consistent with the observed speed range for realistic values of the infant mortality, and (ii) the role of the infant mortality should be taken into account in order to understand human invasion front speeds, as done here for the first time. In figure 1 we also note that the speed decreases with increasing values of the mortality, as was to be expected intuitively (if fewer people survive, fewer people can migrate and the front speed should be slower). Also, according to figure 1, the higher the value of the adult persistence ($p_{e2} = p_{e3}$), the more slowly the front propagates, as was again to be expected (fewer people migrate if the persistence is higher; see section 2). In figure 1 it is also seen that the numerical simulations (circles) confirm the validity of our analytical results (curves).

Finally, in figure 1 we have also included the predictions of the single-population model, i.e. without allowing for any dependences of the fertility, mortality or persistence on age (dashed curve). This is the model corresponding to equation (3) and was analyzed in [14]. Figure 1 illustrates some limitations of the single-population model (dashed curve). Firstly, this model predicts a vanishing front speed if the persistence is equal to 1, because then individuals cannot move at all (in the single-population model, no age dependence of the persistence is possible). In contrast, in the several-population model (full curves in figure 1) the front propagates even if $p_{e2} = p_{e3} = 1$. This is due to the role of $p_{e1} = 0.38 \neq 1$ (see section 3), which appears in the second equation (6). But the most important limitation of the single-population model (dashed curve in figure 1) is that, for a wide range of the persistence, it apparently agrees with the observed Neolithic front speed (hatched rectangle), independently of the value of the infant mortality m_1. The reason is simply that m_1 does not appear at all in the single-population model (equation (3)). In contrast, the several-population model (full curves in figure 1) shows that some values of the infant mortality m_1 are not consistent with the observed speed, a crucial conclusion that a single-population model seems unable to reach.

It is important to estimate the importance of each parameter value for the front speed. In order to do so, in figure 2 we present a sensitivity analysis, performed as follows. All but one of the adjustable parameters were fixed at the characteristic value given in table 1. The speed was then computed for the single remaining parameter set to its minimum and maximum values in table 1. Figure 2 shows that the model is very sensitive to the infant mortality m_1 and, to a lesser extent, to the total fecundity ratio F. The model is somewhat sensitive to the young adult mortality m_2 and to the persistences of the infants (p_{e1}) and young adults (p_{e2}), albeit to a lesser extent. The persistence of the mature adults, p_{e3}, has a non-vanishing but very small effect. Finally, the model is insensitive to the mortality of mature adults, m_3. This was expected because, according to the ethnographic data [32], the oldest individuals (with density p_4) do not reproduce ($f_4 = 0$), so the last equation in the set (5) should not affect the propagation behavior of the front, and it is only in this equation that the parameter m_3 appears. Indeed, this expectation has made it possible to reduce equations (5) to the simpler system (6), which in turn has led us to our analytical result for the front speed (equations (10)–(14)).

Let us analyze in more detail the effect of infant mortality m_1 on the invasion front speed, given its importance (figure 2) as well as its novelty. Figure 3 shows this effect

J. Stat. Mech. (2010) P11006

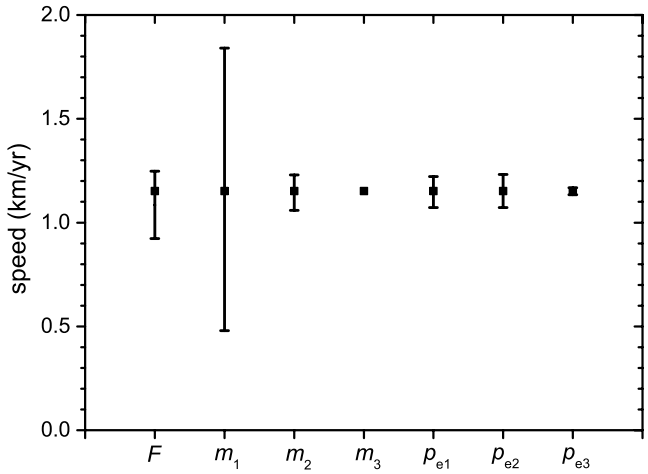

Figure 2. Sensitivity analysis of the model as regards its parameter values (total fertility ratio F, mortalities m_1, m_2, m_3 and persistences p_{e1}, p_{e2}, p_{e3}). The mortality and persistence of the oldest age group (m_4 and p_{e4}, respectively) are not included because they do not have any effect on the front speed (see the main text). The baseline case (squares) corresponds to the characteristic values of the parameters in table 1. Bars show the variation of the front speed about the baseline case for the parameter ranges in table 1.

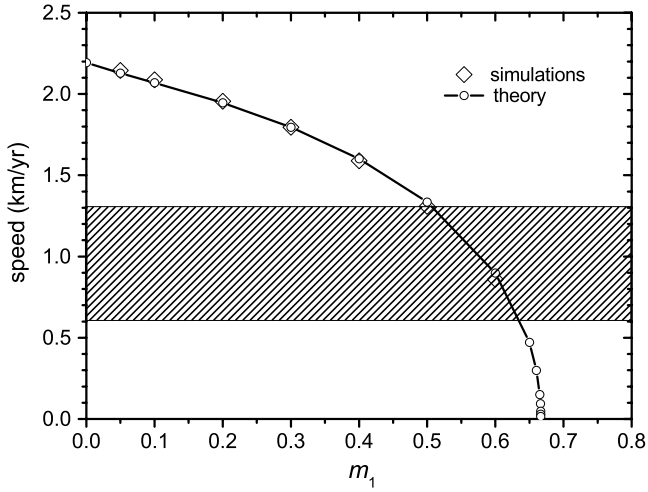

Figure 3. The effect of infant mortality on the speed of the Neolithic transition. The hatched region indicates the observed speed range of the Neolithic transition in Europe [34]. The numerical results (rhombus) agree perfectly with the analytical ones (open circles and full curve). The range of infant mortality consistent with the observations is $0.5 < m_1 < 0.63$.

(when keeping the other parameters fixed at their baseline or characteristic values in table 1). As in figure 1, the hatched rectangle shows the observed speed range for the Neolithic transition in Europe (0.6–1.3 km yr^{-1}). Simulated values (rhombus) are in almost perfect agreement with theoretical ones (open circles and full curve). It is

important to note that, according to figure 3, for the predicted speed to lie within the experimental range, the infant mortality must be rather high, $m_1 > 0.5$. Interestingly, high values of m_1 are indeed observed in pre-industrial populations [32]. However, above a threshold value ($m_1 \simeq 0.63$ in figure 3) infant mortality is too high and the speed too slow compared to the ranges implied by the archaeological data (hatched rectangle). For even larger values of infant mortality, the front speed drops until it vanishes, thereby leading to a front propagation failure induced by infant mortality.

Although we have illustrated our model for a specific application (the Neolithic transition in Europe), clearly it can be also useful for other population expansions. Moreover, the effect of the mortality shown in figure 3 could be related to several interesting factors. For example, a region with less natural resources (or a period of drought) could lead to higher values of the infant mortality m_1, and thus to slower speeds (figure 3) or even to the failure of the invasive species (vanishing speed, also seen in figure 3) to successfully colonize the new habitat.

Finally, since our model treats the dispersal, fecundity and mortality of the individuals in different age groups independently, there is the possibility that the leading edge of the front is dominated by a particular age group. In order to analyze this, in figure 4(a) we plot the age group density profiles as a function of position. Note that for the parameter values used in figure 4 the simulated front speed is about 1.1 km yr^{-1} (from the circles with $m_1 = 0.55$ in figure 1), so at the final time $t = 2500$ yr the front position (defined in section 3 as that with $p_1 = 0.05$) should be about $2500 \times 1.1 = 2750$ km. This is in fair agreement with figure 4(a) (in spite of the existence of an initial transient in the simulations, before a constant front speed is attained). Figure 4(b) is a plot of the mean age as a function of position (obtained directly from the profiles in figure 4(a)). It is seen that the mean age decreases as the front leading edge (right-hand side) is approached. This seems reasonable, and could have been expected because the first of equations (5) implies that some newborn individuals (belonging to the age group with density p_1) appear some distance away from the position where their parents used to lie in the previous iteration.

5. Conclusions

In this paper we have analyzed the effect of age-dependent mortality, fecundity and persistence on the invasion speed for populations that spread across a two-dimensional space. Our simulated and analytical front speeds are consistent with each other and, for realistic parameter ranges, with the observed speed of the Neolithic transition in Europe. Predicted speeds fall within the experimental range for realistic values of the infant mortality (e.g., $m_1 = 0.55$), and this conclusion is independent of the adult dispersal persistence (figure 1). The sensitivity of the results has been analyzed, with reference to a baseline case for the parameter values obtained from the ethnographic literature (figure 2). Infant mortality m_1 and total fecundity ratio F have the most important effects. This is the first model that relates the Neolithic front speed to the age-dependent demographic and dispersal parameters of the population. We have found that there is a relatively narrow range for the value of the infant mortality ($0.5 < m_1 < 0.63$) consistent with the observed range of the Neolithic front speed (figure 3). Of course, more complicated models can be considered, but for the application considered here it is very difficult to

J. Stat. Mech. (2010) P11006

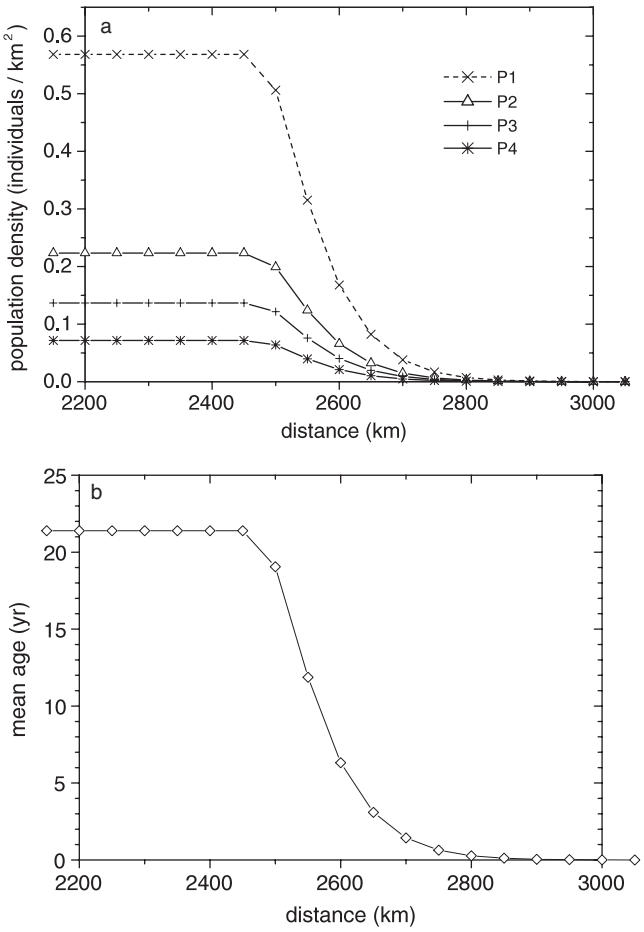

Figure 4. (a) Age profiles of the Neolithic subpopulations (p_1, p_2, p_3 and p_4 correspond to the population densities of age groups with mean ages 12.5 yr, 25 yr, 37.5 yr and 50 yr, respectively). The saturation density of the total population ($p \equiv p_1+p_2+p_3+p_4$) is reached for $p = p_{\max} = 1$ individuals km^{-2} (corresponding to $50^2 = 2500$ individuals per square cell with side 50 km). We have used the characteristic values in table 1 for m_i and p_{ei}, the values in section 3 for f_i ($i = 1, 2, 3, 4$) and a final time $t = 200$ iterations $\cdot$ 12.5 yr/iteration $= 2500$ yr. (b) Mean age of the Neolithic individuals as a function of position, obtained from the plots in 4(a) as $12.5p_1 + 25p_2 + 37.5p_3 + 50p_4$. It is seen that the mean age decreases as the front leading edge is approached.

find more detailed ethnographic data, and our simple model takes into account the age dependence of the major demographic parameters.

This paper opens the way to predicting human invasion front speeds from demographic traits, such as the fertilities and mortalities of age groups. The estimates for such demographic parameters that we have used are based from anthropological data from present pre-industrial agricultural populations. But it is very interesting that Bocquet-Appel and co-workers [35]–[37] have measured the evolution of fertility rates directly from archaeological data (incidentally, this has led to the important proposal that the Neolithic transition was driven initially by increased fertility rates, attributed to a decrease

J. Stat. Mech. (2010) P11006

in inter-birth interval, and followed by increased mortality rates). Such archaeological fieldwork may lead to direct estimates for the demographic parameter values of prehistoric populations necessary for applying our model. Conversely, our model can be also used to constrain demographic traits from measured front propagation rates, and the demographic parameter values thus derived could be compared to those measured directly from archeological data.

References

[1] Fort J and Méndez V, 1999 *Phys. Rev. Lett.* **82** 867
[2] Davison K, Dolukhanov P, Sarson G R and Shukurov A, 2006 *J. Archaeol. Sci.* **33** 641
[3] Fort J and Méndez V, 2002 *Phys. Rev. Lett.* **89** 178101
[4] Fort J, 2007 *J. Appl. Phys.* **101** 094701
[5] Merikoski J, Maunuksela J, Myllys M and Timonen J, 2003 *Phys. Rev. Lett.* **90** 024501
[6] Pujol T, Fort J, González J R, Montoro L and Pelegrí M, 2008 *Physica* A **387** 1987
[7] Fort J and Méndez V, 2002 *Rep. Prog. Phys.* **65** 895
[8] van Saarloos W, 2003 *Phys. Rep.* **386** 29
[9] Fort J and Pujol T, 2008 *Rep. Prog. Phys.* **71** 086001
[10] Steele J, 2009 *Hum. Biol.* **81** 121
[11] Fisher R, 1937 *Ann. Eugenics* **7** 353
[12] Kolmogorov A, Petrovsky J and Piscounov N, 1937 *Moscow Univ. Bull. Ser. Int.* A **1** 1
[13] Isern N and Fort J, 2009 *Phys. Rev.* E **80** 057103
[14] Fort J, Pérez-Losada J and Isern N, 2007 *Phys. Rev.* E **76** 031913
[15] Isern N, Fort J and Pérez-Losada J, 2008 *J. Stat. Mech.* P10012
[16] Murray J D, 1993 *Mathematical Biology* 2nd edn (Berlin: Springer) p 37
[17] Nowak M, 2006 *Evolutionary Dynamics* (Cambridge: Harvard University Press) p 13
[18] Méndez V, Campos D and Fort J, 2004 *Europhys. Lett.* **66** 902
[19] Hall C A S, 1988 *Ecol. Modell.* **43** 5
[20] Neubert M and Caswell H, 2000 *Ecology* **81** 1613
[21] Caswell H, 1989 *Matrix Population Models* (Sunderland: Sinhauer)
[22] van den Bosch F, Metz J A J and Diekmann O, 1990 *J. Math. Biol.* **28** 529
[23] Di Blasio G, 2010 *J. Evol. Equ.* at press, doi:10.1007/s00028-010-0077-8
[24] Amor D R and Fort J, 2009 *Phys. Rev.* E **80** 051918
[25] Brunet E and Derrida B, 1997 *Phys. Rev.* E **56** 2597
[26] Doering C R, Mueller C and Smereka P, 2003 *Physica* A **325** 243
[27] Fort J, Pérez-Losada J, Suñol J J, Escoda L and Massaneda J M, 2008 *New J. Phys.* **10** 043045
[28] Ebert U and van Saarloos W, 2000 *Physica* D **146** 1
[29] Sellen D W and Mace R, 1997 *Curr. Anthropol.* **38** 878
[30] Bogin B, 2001 *The Growth of Humanity* (New York: Wiley-Liss)
[31] Galeta P and Bruzek J, 2009 *Doc. Praehistorica* **36** 139
[32] Eshed V, Gopher A, Gage T B and Hershkovitz I, 2004 *Am. J. Phys. Anthropol.* **124** 315
[33] Stauder J, 1971 *The Majangir. Ecology and Society of a Southwest Ethiopian People* (Cambridge: Cambridge University Press)
[34] Pinhasi R, Fort J and Ammerman A J, 2005 *PLoS Biol.* **3** 2220
[35] Bocquet-Appel J P, 2002 *Curr. Anthropol.* **43** 637
[36] Bocquet-Appel J P and Naji S, 2006 *Curr. Anthropol.* **47** 341
[37] Bocquet-Appel J P, 2009 *Curr. Anthropol.* **50** 657

J. Stat. Mech. (2010) P11006